PROCEEDINGS, 42nd Workshop on Geothermal Reservoir Engineering
Stanford University, Stanford, California, February 13-15, 2017
SGP-TR-212

The use of ^{222}Rn to Constrain Fracture Characteristics: Experiments Conducted at the Meso-Scale Model Geothermal Reservoir Site at Altona, New York

John N. Christensen[1a], Adam Hawkins[2b], Shaun T. Brown[1c], Eric Sonnenthal[1d], Neil Sturchio[3], and Donald J. DePaolo[1]

[1]Lawrence Berkeley National Laboratory, 1 Cyclotron Rd., Berkeley, CA 94705

[2]Cornell University, Cornell Energy Inst., Ithaca, NY 14850

[3]Univ. of Delaware, Dept. Geological Sci.s, 255 Academy St., Newark, DE 19716

[a]jnchristensen@lbl.gov; [b]ajh338@cornell.edu; [c]stbrown@lbl.gov; [d]elsonnenthal@lbl.gov

Keywords: ^{222}Rn, field experiment, fracture aperture

ABSTRACT

^{222}Rn, a noble gas with a half-life of 3.8 days produced in the decay-chain of ^{238}U, has the potential to provide constraints on the aperture and surface area of fractures prior to and after EGS stimulation. In order to test and better understand the use of ^{222}Rn in geothermal settings, we have conducted tests at the Altona, NY model geothermal reservoir. The experimental site is situated on an expanse of exposed quartz-cemented Cambrian sandstone with <1% porosity, with permeability dominated by bedding parallel fractures. A well field provides access to a through going near-horizontal fracture at 7.6 m depth that conducts water from a nearby lake (an effectively zero ^{222}Rn water source) and has been previously used for tracer and heating experiments (Hawkins et al. 2015). Groundwater from the fracture has ^{222}Rn concentrations up 2100 pCi/L, and depends on flow rate. Using the ^{222}Rn concentration at a natural seep ~75 m down-gradient from the well field, we estimate a fracture aperture of ~0.5 mm, in rough agreement with estimates by other means (Hawkins et al. 2015). In the conducted experiments we used a tank of groundwater that had been stripped of ^{222}Rn and spiked with iodide and Cs tracers. This was injected and tracer breakthrough and ^{222}Rn concentrations were measured in a monitoring well approximately 14m from the injection well. The results of the experiment have been modeled with the ToughReact THMC model that supports the earlier work, and suggests a secondary source of ^{222}Rn was accessed.

1. INTRODUCTION

The goal of Enhanced Geothermal System (EGS) technology is the production of efficient fluid/rock heat exchange through the creation of increased fracture surface area with a narrow range of fracture apertures. To fully evaluate the results of an EGS technology application, a comparison is necessary of the pre- and post-stimulation natures of the fracture network- including fracture surface area, spacing and fluid transit time. One avenue for the development of approaches to this problem is the use of isotopic techniques, taking advantage of natural isotopic variations of rocks, minerals and fluids to interrogate the system. An example of this is the modeling of the strontium and oxygen isotopic compositions of rock and fluids in mid-ocean ridge hydrothermal systems to extract the spacing of fluid-bearing fractures (DePaolo 2006). Most isotopic systems reflect slow equilibration between the rock matrix and advecting fracture fluids with the implication that fracture fluid isotopic compositions are relatively insensitive to the fracture surface area and aperture (Brown et al., 2013). Here we explore the use of ^{222}Rn, a relatively short lived naturally occurring isotope of radon, to obtain information on fracture surface area and aperture in EGS through field observations and experiments at the ambient-temperature model hydrothermal site at Altona, NY. The short half-life of ^{222}Rn means that only radon produced near the fracture surface can be added to the fracture fluid by direct emanation or aqueous diffusion. We use the ToughReact THMC model to explore the behavior of ^{222}Rn in this simple system and to extrapolate and forecast the potential of the use of ^{222}Rn in EGS to evaluate fracture properties.

^{222}Rn is a naturally occurring radioactive isotope in the decay chain of ^{238}U, and has a half-life of 3.82 days decaying to its daughter ^{218}Po. Its immediate parent ^{226}Ra has a half-life of 1600 yrs. The chemical behavior of radon (Rn) and radium (Ra) are quite distinct, with Rn behaving as a noble gas exhibiting a greater affinity for fluids over solids (and for air over water) while Ra has chemical similarities with Ca and can be incorporated into mineral precipitates. This contrast in behavior can lead to chemical separation of Rn and Ra, and so radioactive disequilibrium between ^{226}Ra and ^{222}Rn.

A very simple model, illustrated in Figure 1 and described by Eq. 1, provides the connection between the concentration of ^{222}Rn in the fluid held in fracture and the fracture aperture (Nelson et al. 1983):

$$C_{Rn} = E/(\lambda \bullet h) \quad (1)$$

where C_{Rn} is the ^{222}Rn concentration in the fluid occupying the fracture, E is the emanation rate of ^{222}Rn (atoms per cm^2, per sec), λ is the decay constant (sec^{-1}) of ^{222}Rn, and h is the fracture aperture (cm). In this simple model, it is assumed that the residence time of fluid in the fracture is long compared to the 3.8 day half-life of ^{222}Rn, and in order to calculate fracture aperture, the ^{222}Rn emanation rate needs to be constrained. In the experiments described below the groundwater residence time is short compared to the ^{222}Rn half-life, but can be accounted for in the numerical model we use to evaluate the measured ^{222}Rn concentrations in the tracer experiment described below. The second issue is the emanation rate of ^{222}Rn to the fracture water. Previous workers in interpreting ^{222}Rn data, use the bulk concentration of ^{238}U in the rock containing the fracture to calculate the emanation from the fracture surface. Sometimes this

has given reasonable results, but often this has under predicted the fluid ^{222}Rn activity, suggesting a greater concentration of the parent(s) of ^{222}Rn at the fracture surface than would be expected from the bulk concentration of ^{238}U or ^{228}Ra in the rock. Solutions proposed to explain the discrepancy include mineral coatings on fractures with higher ^{238}U or ^{228}Ra concentrations, or enhanced surface areas by nanoporous materials in the near fracture environment (Porcelli et al. 2003). Our approach to this problem is to model our observations of the increase in ^{222}Rn concentration between Chasm Lake (the groundwater source) and groundwater from the well field to derive a consistent value for the emanation rate.

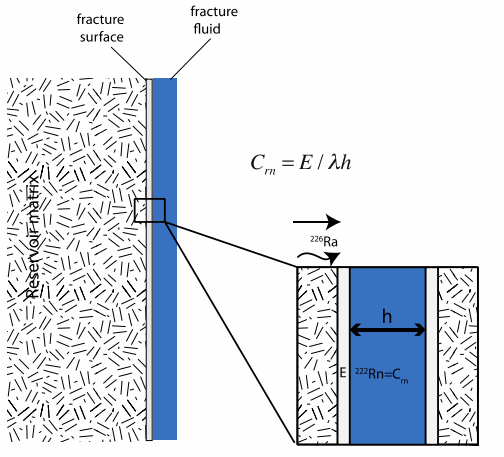

Figure 1: Cartoon showing the simple model of ^{222}Rn emanation from a fracture surface into the fluid occupying the fracture volume. As fracture aperture, h, increases the steady state ^{222}Rn concentration in the fluid decreases.

2. THE ALTONA EXPERIMENTAL SITE

The experimental site is situated in the Altona Flat Rock, in northern New York State, USA about 6 km northwest of West Chazy. The Altona Flat Rock is a sub-horizontal expanse of Cambrian aged Potsdam Sandstone, stripped of soil by catastrophic glacial floods ~1200 yrs ago, representing a unique Jack Pine forest ecosystem in the Northeastern United States (Rayburn et al., 2005). The Potsdam Sandstone is well cemented with silica and as a consequence has a matrix (or "primary") porosity of roughly 1 percent. Ubiquitous fracturing, however, makes the formation highly permeable and it is commonly contains shallow, fracture-hosted aquifers exploited locally for drinking water (Olcott, 1995).

The Altona Flat Rock site where our experiments were conducted is located in the William H. Miner Experimental Forest (http://www.whminer.com/). The experimental site was selected for its lack of soil cover, the shallow water table, and the presence of strong sub-horizontal bedding plane fracturing. Reconnaissance Ground Penetrating Radar (GPR) surveys located a reflection at 7.6 m depth that was interpreted to be an open bedding plane fracture. Subsequent drilling of a well field in 2004 confirmed the location of a permeable fracture that was suitable for conducting tracer and hydraulic testing. Since the drilling of the wells, multiple experiments have been carried out at the site to investigate flow and solute transport (Hawkins et al. 2016, and references therein).

The well field is located near an abandoned dam (Skeleton Dam) which creates a hydraulic gradient of roughly 0.004 [-] across the well field as water flows from the artificial reservoir (Chasm Lake) to a small ledge which produces a seepage face (Figure 2) (Becker and Tsoflias, 2010). A five-spot 15 cm diameter well pattern penetrates a conductive sub-horizontal fracture 7.6 m below the surface. Transmissivity of the fracture is estimated to be about 5 m^2/day which suggests a mean hydraulic aperture of roughly 0.5 mm based upon an analysis of slug tests performed at the Altona well field (Talley et al., 2005).

The wells of the five-spot configuration, drilled using a water rotary drill in May of 2004, are 15 cm in diameter and were originally drilled to a depth of 12.2 m with a 0.91 m surface casing and open borehole below. In July of 2011, all five wells were deepened with a percussion air rotary drill with a 14 cm diameter bit. The new well depths ranged from 18.3 m to 21.3 m. PVC casings were installed from ground surface to roughly 0.7 m below surface. An open borehole in the sandstone rock remained below the bottom of casing. Roughly 15 to 30 cm of PVC casing was left exposed above ground surface. Bentonite clay was used to seal the casings to the formation.

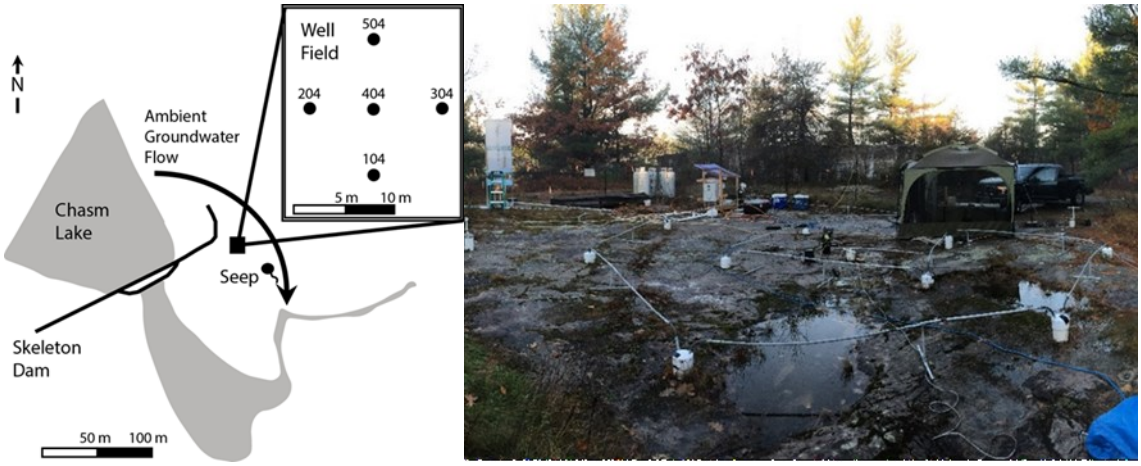

Figure 2: Map of the Altona field area and well field (left) and a photograph of the wellfield taken in October 2016 (right). In photo, the tank that held the tracer injectate is to the upper left. The injection well is near the small lean-to to the right of the injectate tank, while the production well is the short-white cylinder at the far right.

3. FIELD EXPERIMENTS AND SAMPLING

Over the course of two field visits (in Oct. 2015 and July 2016) several different experiments and measurements were performed. The Oct. 2015 campaign included background sampling of well 304 (Fig. 2), Chasm Lake and a nearby seep (Fig. 2), as well as a tracer experiment using extracted groundwater that had been partially de-gassed of ^{222}Rn (by ~50%). With this particular experiment we experienced some difficulty maintaining constant flow, and our method of degassing (spraying the water while filling the source tank with groundwater) was only partially successful in removing dissolved ^{222}Rn from the injectate, and hence this experiments will not be discussed further in this report. We returned in July 2016 for a second, more successful set of experiments.

In addition to water sampling, we collected for elemental, mineralogical and textural analyses a set of outcrop samples of sandstone from a nearby ledge, as well as core samples taken at the well plot.

3.1 Tracer and Pump Tests (July 2016)

A pump test was conducted two days prior to the tracer test. In this experiment, groundwater was pumped from the production well without tracer injection in order to examine the effect on measured ^{222}Rn. After pumping for 11 minutes, 21 samples were collected for ^{222}Rn analysis over the subsequent 147 minutes of pumping. After about 105 minutes, reinjection of the produced groundwater was started.

Tracer testing was conducted under forced convection conditions between an injection and production well. Flow was induced by a variable speed positive displacement pump (Rediflow-2, Grundfos). Production water was directly re-injected into the injection well (well 204, Fig. 2) after circulating through a tankless water heater (in this test there was no heating). The injection and production volumetric flow rates were 5.7 and 6.8 L/min, respectively. Injection and pumping were conducted from a hydraulically isolated zone in the wellbores that were aligned with the 7.6 m deep test fracture. Hydraulic isolation in the injection well, pumping well, and three observation wells was achieved using two modified inflatable pipe packers (Lansas Products, Lodi, California) in each well and the vertical spacing in the wells between the two packers ranged from 0.2 to 0.5 m.

Tracer injection was performed as a "step" test configuration in which a constant-concentration tracer was continuously injected into the injection well for the duration of the experiment. The tracers included Cesium and Iodide that were introduced as a CsI salt into a 650 L tank filled with groundwater pumped from the well field. The Iodide and Cesium concentrations injected were 0.21 and 0.18 ppm, respectively. To effectively scrub the tracer water of ^{222}Rn prior to injection, an air pump was used to force air through a pair of showerheads submerged near the bottom of the tank. Air was bubbled through the tank for ~10 hours, and resulted in measured ^{222}Rn concentration of 30 pCi/L, a factor of 70 lower than background. This process also raised the O_2 concentration of the injectate from ~0.2ppm to saturation (8.3 ppm at the measured temperature of 25˚C), providing an additional tracer of the injectate. During the experiment, several different sample types were collected from the production well (well 304, Fig. 1). For Cs and I analysis, samples were collected in 15 mL High-Clarity Polypropylene Conical Tubes (Corning ©) and immediately stored in ice water where they remained until they were analyzed. Samples for ^{222}Rn concentration analysis were collected in either 40ml or 250ml glass bottles, and analyzed within 48hrs.

3.2 Analytical Techniques

Analysis of Iodine and Cesium tracer concentrations were performed using inductively coupled plasma mass spectrometry (Element 2^{TM} ICP-MS, Thermo Fischer Scientific Inc., MA, USA). The concentration of ^{222}Rn was determined in water samples using a RAD7 (Durridge Co., Massachusetts, USA) portable radon detector with the RAD H2O kit. Measured ^{222}Rn concentrations were corrected for decay to the time of sample collection. During the tracer experiment, dissolved Oxygen concentration was measured every two minutes using an in-line meter and data logger. Included was measurement of water temperature, pH and ORP.

4. RESULTS

The results of the pump test of July 26, 2016 are presented in Fig. 3, displaying against time the measured ^{222}Rn concentrations of samples collected during the experiment. The average ^{222}Rn concentration of all 22 samples taken during the tes is 2136±51 (95% confid.) pCi/L. The average ^{222}Rn of the samples taken before reinjection began is 2123±81 (95% confid.) pCi/L, which is indistinguishable with the average, 2151±59 (95% confic.) pCi/L, of the samples taken after reinjection. This suggests that simply pumping on the aquifer for over 100 minutes has no appreciable effect on the ^{222}Rn concentration of the produced water. We take a ^{222}Rn concentration of 2136±51 pCi/L (the average of all the samples) to represent the steady state background concentration at the time of the tracer test conducted on July 28.

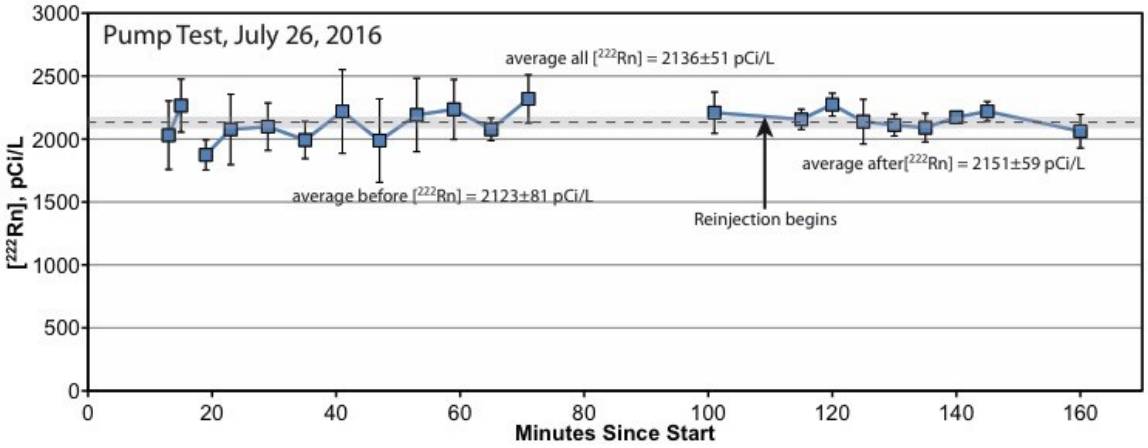

Figure 3: The ^{222}Rn concentrations of samples collected during a pumping test plotted against time. At ~115 minutes, reinjection of the produced groundwater was started. Dashed line represents the average ^{222}Rn concentration of all the samples.

The results of the tracer test conducted on July 28, 2016 are presented in Figures 4-5. The Iodine, Cesium and Oxygen tracer recover is shown Fig. 4. The first arrival of the injectate is first apparent in the dissolved oxygen (DO) concentration at ~12 minutes after the initiation of injection, rising quickly between 12 and 24 minutes, to 60% of the injectate concentration, and then more slowly between 24 and 80 minutes at which time the DO concentration reached about 80% of the injectate concentration. Seven minutes after the end of injection, the DO concentration of the produced water peaked at 97% of the injectate, before falling off to the background concentration over the next 40 minutes. In contrast, neither the Iodine or Cesium tracers behaved conservatively, but did follow the pattern of the DO concentration (better seen in Fig. 4 where absolute concentrations have been plotted). The maximum in I peaked at 24% of the injectate concentration, while Cs reached only 7% with a muted peak. It's likely that the I^- and Cs^- were absorbed by mineral surfaces, while DO appears to behave essentially conservatively at the time scale of the experiment, despite its potential reaction by presumably reduced minerals in the aquifer.

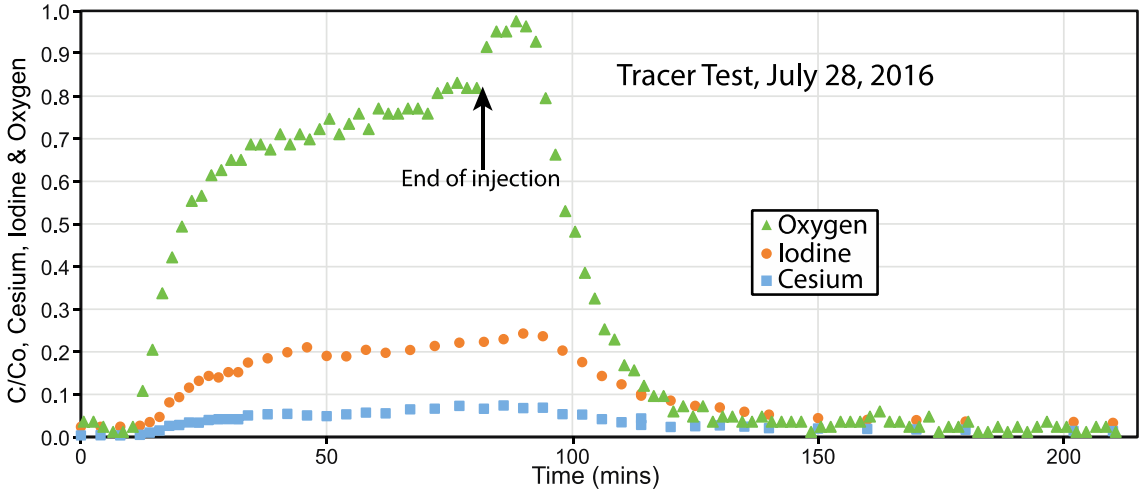

Figure 4: The ratio C/Co versus time for Cesium, Iodine and dissolved Oxygen (DO) in produced groundwater during the tracer experiment. Co for iodine = 200.2 ppb, Co for cesium = 175.9 and Co for DO = 8.3 ppm based on the measured injectate temperature of 25°C.

The measured concentrations of ^{222}Rn in samples collected during the tracer test are compared to the concentrations of Cs, I and DO in Figure 5. The curves for I and DO are similar in shape, peaking at approximately the same time given their slightly different sampling intervals. The DO concentration curve rises slightly faster, and falls off faster than the I curve, consistent with the less conservative

behavior of I. As indicated above (cf. Fig. 3), Cs exhibits even greater deviation from conservative behavior. The peak in DO occurs about 7 minutes after the injectate was halted and the reinjection of produced water was begun (the switchover took a couple of minutes). The ^{222}Rn concentration follows a very different pattern than the DO concentration. About 7 minutes after the start of the rise in DO, there is only a modest drop in ^{222}Rn concentration, with an average concentration of 1824±36 pCi/L between 20 and 50 after injection began, compared to the background concentration of 2136±51 pCi; a difference of 312±62 pCi/L. However, at the peak in DO concentration at the 88th minute, the ^{222}Rn concentration drops to 115±29 pCi/L. Subsequent to that, the ^{222}Rn rises back to an average concentration of 2117±130 pCi/L, within error of the background concentration, while the DO returns to the background value.

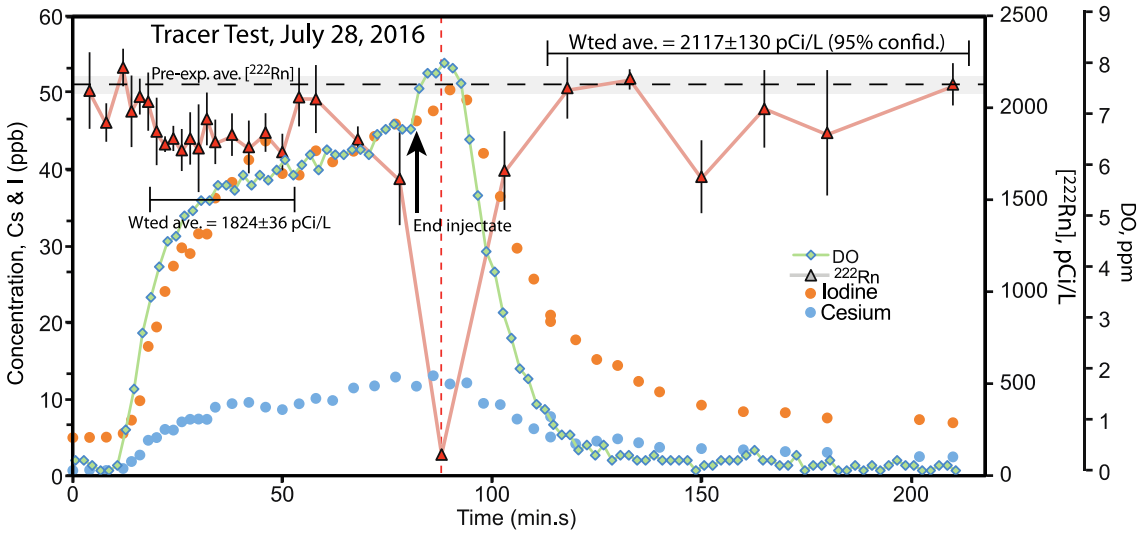

Figure 5: Concentrations of Cs (blue circle) and I (orange circles) given by the left hand axis; concentration of ^{222}Rn (red triangles) given by the scale on the right; concentration of dissolved oxygen (green diamonds) given by the far right scale. The arrow indicates the time when the injection of the injectate was halted and the recirculation of produced water was started. The dashed line and grey bar represents the average and ±95% confidence interval of the concentration of ^{222}Rn measured in samples taken during the pumping test on July 26.

In Figure 6 we present a very simple mixing model for ^{222}Rn concentration in the produced groundwater. We use the background and injectate concentrations to calculate the fraction of injectate for each measured sample DO concentration. We then use this calculated fraction of injectate, along with the background and injectate ^{222}Rn concentrations (2136 and 30 pCi/L) to calculate the ^{222}Rn concentration in the mixture represented by each sample. This simple mixing model appears to capture the low point in ^{222}Rn concentration and the recovery of the ^{222}Rn, but does not replicate the ^{222}Rn concentrations seen in the earlier (the period of 12-80 minutes after injection) portion of the experiment. It appears that a secondary source of ^{222}Rn is needed to maintain the ^{222}Rn concentration. This is explored further below with reactive transport modeling.

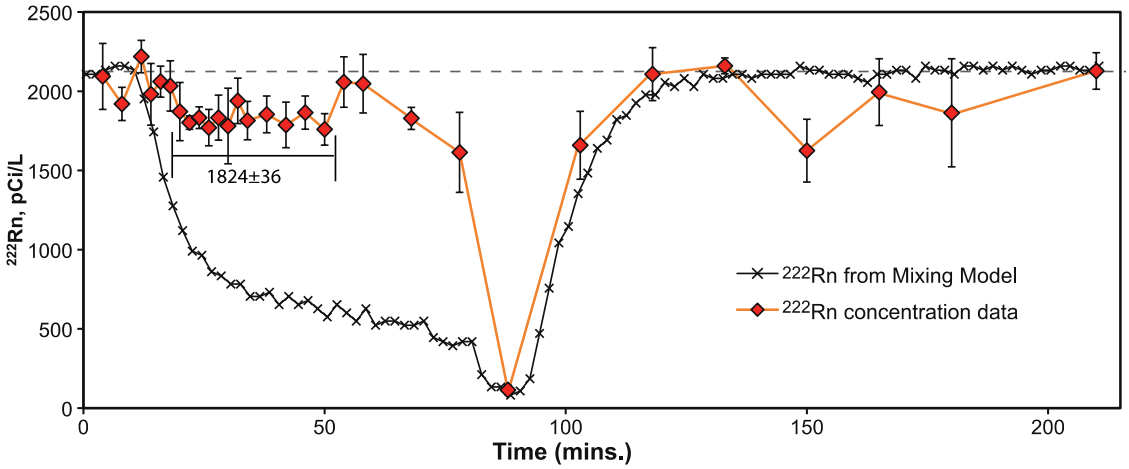

Fig. 6: Comparison of a simple mixing model for the ^{222}Rn concentration in the produced groundwater compared to the actual measures ^{222}Rn concentrations. The mixing model is based on measured DO concentrations and is described in more detail in the text.

5. REACTIVE TRANSPORT MODELING

Radon levels in groundwater from fractured rocks are known to be highly variable, and within a given rock type are not directly related to uranium abundances (Torgersen et al., 1990). This variability has been shown to be partially a function of fracture aperture (Torgersen et al., 1990), but also strongly affected by radium abundances (^{226}Ra) on fracture surfaces, which may be in excess of that expected for secular equilibrium with bulk ^{238}U in the rock (Wood et al., 2004). The latter authors demonstrated radium buildup on fracture surfaces owing to matrix diffusion and sorption (or ion exchange) on secondary minerals at the fracture surface. Water chemistry (redox state) also plays a role in radium sorption and transport (secondary to initial uranium abundance), also affecting radon activities in groundwater (Vinson et al., 2009).

Preliminary reactive transport modeling was performed to investigate whether fracture surface areas and aperture could be determined through radon measurements at the Altona site. Radon activities were measured in the pumping well (Well 304) prior to injection as well as during injection and pumping. Uranium measurements on whole rocks (surface collected) were found to be in the range of 1-4 ppm. However, no radium measurements have been performed and the only other measurement of radon activity comes from a seep located about 117 meters down gradient from Well 304.

^{222}Rn generation rates and transport were evaluated using a 2-D model from the lake edge (dam face) to the seep location and also in 3-D model of the experimental site. The lake to seep model was developed to evaluate the hypothesis that water in the well field was predominantly sourced from Chasm Lake, located up gradient about 64 meters from Well 304. A hydraulic gradient of about 0.004 and an average background flow velocity of 0.0022 m/s (Hawkins et al., 2016) were used to evaluate fracture permeabilities at the large scale (181 meters from lake edge to seep). At the well field scale (~26 m), the porosity and permeabilities were varied to capture tracer concentrations, since the apertures were shown to be highly variable and a channel of large aperture was observed (Hawkins et al., 2016) between the injection well (Well 204) and Well 304, only 14 m apart (Table 1). The channeled flow was approximated by using anisotropic permeabilities in the fracture plane, with k_x twice that of k_y.

Two cases are shown (among many tested), with the second case closer to a cubic law permeability (with roughness factor of 1.5) giving higher steady-state flow rates than the observed average rate (0.0022 m/s). As expected, varying matrix permeabilities had virtually no effect on the results, given the roughly 4-6 orders of magnitude higher fracture permeability.

Parameter	Fracture (L-S)	Sandstone (L-S)	Fracture Case 1	Sandstone Case 1	Fracture Case 2	Sandstone Case 2
ϕ	0.125	0.01	0.115	0.01	0.15	0.01
k_x (m^2)	9.34×10^{-9}	10^{-16}	6.24×10^{-9}	10^{-15}	2.0×10^{-8}	10^{-15}
k_y (m^2)	9.34×10^{-9}	10^{-16}	3.12×10^{-9}	10^{-15}	1.0×10^{-8}	10^{-15}
k_z (m^2)	10^{-16}	10^{-16}	10^{-15}	10^{-15}	10^{-15}	10^{-15}
Aperture (mm)	0.50	-	0.46	-	0.6	-
τ	1.0	1.0	1.0	1.0	1.0	1.0
Rn flux/mol U (mol/kg H_2O/s)	10^{-14}	10^{-14}	10^{-14}	10^{-14}	3×10^{-14}	3×10^{-14}

Table 1: Hydrological and Transport Parameters for Lake-Seep (L-S) and 3-D Site Model (Case 1 & 2 Parameters)

The model grid considers a 4 mm wide zone containing a fracture that was varied in aperture from 0.46 mm to 1 mm (in the range of those determined by Hawkins et al., 2016) through modification of the porosity (Figure 7). Two bounding matrix block thicknesses were considered (0.048 m and 0.498 m) to capture fracture-matrix interaction owing to diffusion and potentially pressure-induced flow during injection/pumping.

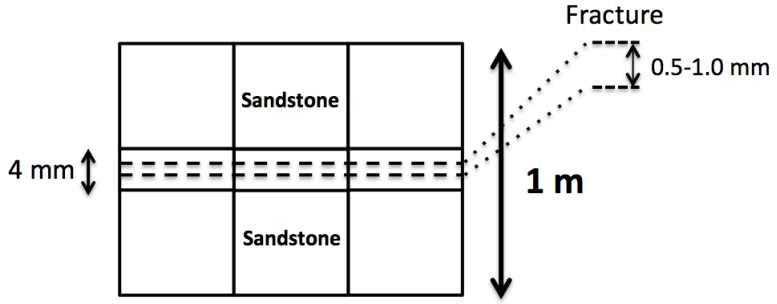

Figure 7: Schematic diagram of the numerical model showing fracture zone and bounding rock matrix grid blocks (not to scale).

TOUGHREACT V3.3 was used for reactive-transport simulations (Sonnenthal et al., 2014; http://esd1.lbl.gov/research/projects/tough/software/toughreact.html; Xu et al., 2011). TOUGHREACT V3.3 considers kinetic and equilibrium mineral-water-gas reactions, radioactive decay, and variable aqueous diffusion coefficients for uncharged and trace species, along with multiphase fluid and heat flow. All simulations were performed assuming fully water-saturated conditions using the EOS1 (pure water) equation-of-state module. The grid dimensions are 1 m in the X-direction (flow direction) for the lake-seep model and

0.3048 m (in X- and Y) for the 3-D well-field model). Time steps were limited using a Courant condition of 0.5 on the fastest flow velocity which is required for accurate results for strong advective flow coupled to ^{222}Rn generation and decay.

The geochemical model considers a rock consisting solely of quartz with a U abundance of 4 ppm (using a solid U volume fraction equivalent to 4 ppm U). The injected tank water was equilibrated with atmospheric O_2 and CO_2 to determine the O_2 (aq) and HCO_3^- concentrations in the injection fluid, since the tank water (groundwater) had been flushed with air continuously for several hours to scrub dissolved radon. The model for ^{222}Rn generation uses a first order reaction rate for ^{238}U in the solid decaying to ^{222}Rn added to the water (assuming secular equilibrium). The effective addition rate of ^{222}Rn to water (mol s^{-1} kg^{-1} H_2O) was calibrated starting with the flux due to ^{238}U decay. Depending on the flow rate and porosity assumed for the fracture this gave effective fluxes of ^{222}Rn to the pore fluid in the range of 10^{-21} to 10^{-23} mol s^{-1} kg^{-1} H_2O. Diffusion of O_2 (aq) and ^{222}Rn (aq) were given temperature-dependent diffusion coefficients, however they were essentially constant at approximately 1 x 10^{-9} m^2/s at the nearly constant groundwater temperature of 10.5 °C. A steady-state simulation was first run for all cases including fracture-matrix diffusion, ^{222}Rn generation, advection, and decay under the imposed 0.0037 hydraulic gradient. The steady-state flow and concentration field was then used as initial conditions for the pumping/injection run.

Modeled ^{222}Rn activities in groundwater as a function of distance from the lake edge are shown in Figure 8. Note the large activity gradient from the lake to the seep and the calibrated activity of Well 304 crossing the range of background measurements. Unfortunately, the only other data point is from the seep that was taken in a prior year when the lake level was higher, and thus the local hydraulic gradient. This value is much lower than the model predicts, questioning the conceptual model of flow directly from the lake and the flux gradient. Since there are no other data for which to calibrate the background ^{222}Rn fluxes to groundwater, this was the starting point for the 3-D well field model denoted also on Figure 8. Another interesting of the gradient model is that the ^{222}Rn activities at injection Well 204 are about 500 pCi/liter lower that at Well 304, even though they are only 14 meters apart. Certainly, data from this and other wells would be needed to test the model.

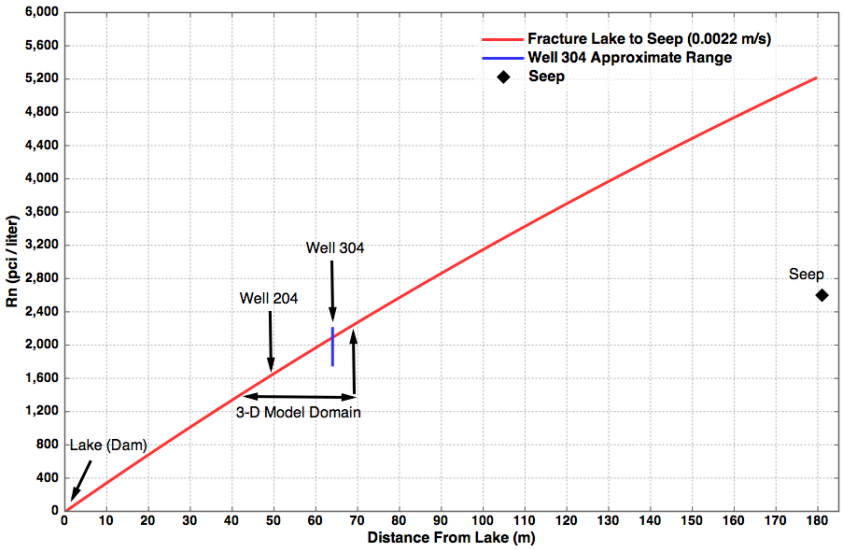

Figure 8: Simulated Lake Chasm to seep radon activities (pCi/liter) assuming a radon activity near zero for lake water and effective radon matrix-fracture water addition rates (effectively the "emanation rate"), calibrated to Well 304 radon activities of about 2100 pCi/liter.

The experiment was modeled in 3-D with injection and pumping rates of 5.7 liters/minute and 6.78 liters/minute, respectively. The tank water injected into Well 204 contained Cs and I reactive tracers, but no conservative tracers. Given that sorption of Cs and I are related both to the sorption coefficients and abundances of the fracture surface minerals (both unknown), and the fracture surface areas, they cannot be used to determine unique fracture properties, so we only modeled them as conservative tracers for these simulations. O_2 (aq) is probably the closest to a conservative species that was measured in the pumped fluid, however the injectate concentration was not measured prior to injection. Whereas the peak O_2 (aq) concentrations observed (about 8.1 ppm) suggest equilibration with air at about 25 °C (the measured temperature of the injectate in the tank before the start of injection), this value would require a lack of significant mixing, and no loss due to oxidation, which is unlikely given the reducing conditions in the groundwater. It's possible that the actual oxygen concentration in the injectate may have been higher as a result of introduced air bubbles and equilibration at a lower temperature after flowing through the pump. Therefore, the injection water was equilibrated with air (O_2 and CO_2) at the same temperature as the groundwater (10.5 °C).

Results for the distribution of ^{222}Rn Case 2 distributions are shown in Figure 9 after 10 and 60 minutes of pumping and injection. The initial high gradient in ^{222}Rn activities can be seen at the top and bottom boundaries. Well 304 pumps in downstream higher activity waters with upstream low activity waters, allowing for the observed relatively high ^{222}Rn activities. The lower set of figures show the distribution after re-circulating groundwater with a ^{222}Rn activity of 2200 pCi/liter. The re-circulated composition is unknown and TOUGHREACT cannot re-inject pumped waters, so just groundwater was re-injected.

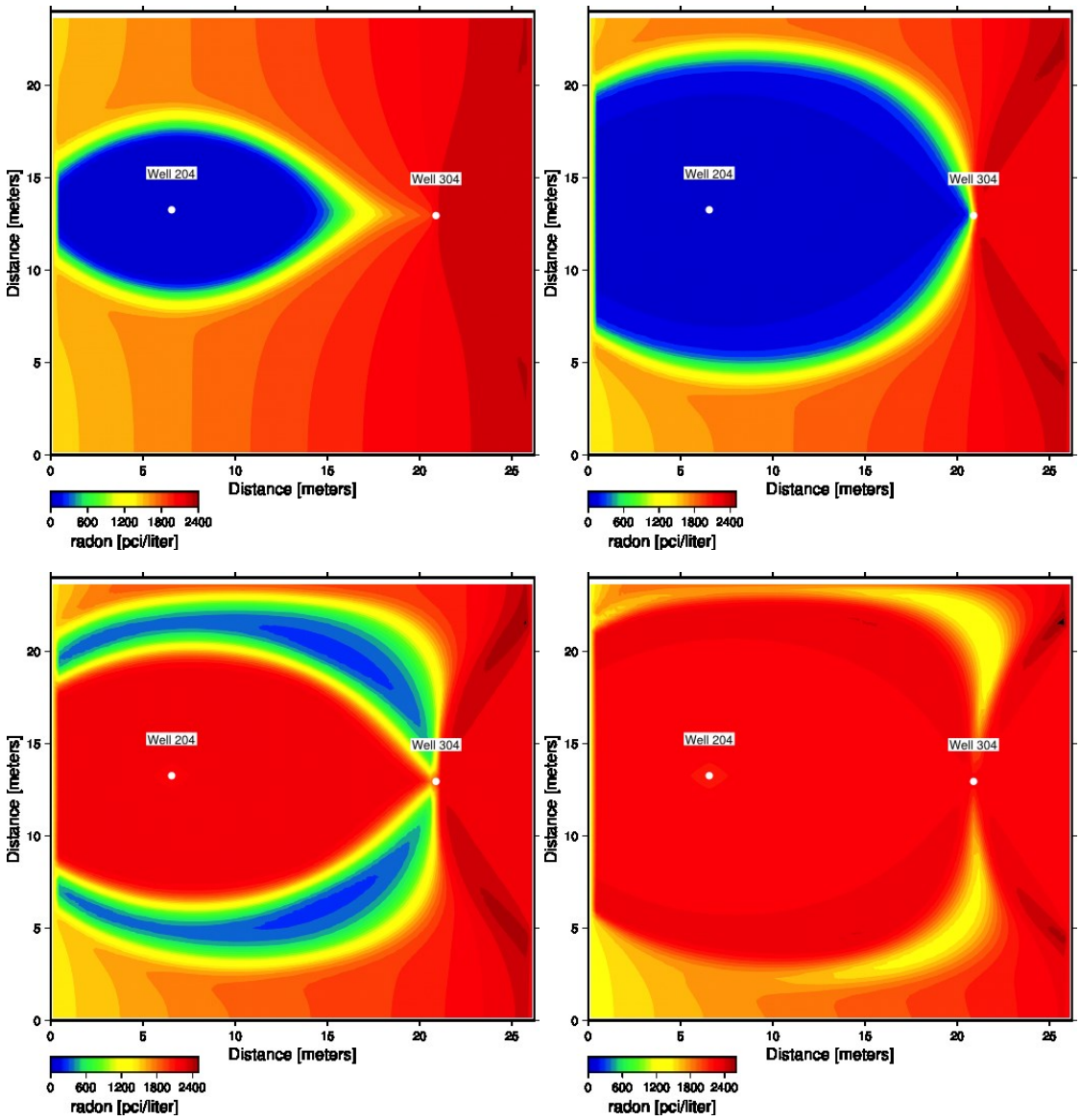

Figure 9: Distribution of ^{222}Rn activities (pCi/liter) for Case 2 hydrologic properties after 10 minutes (upper left) and 60 minutes (upper right) of pumping from Well 304 and injection into Well 204. Plots of the recirculation period are shown at the lower left (120 minutes) and lower right (220 minutes). Boundary conditions are fixed pressure on the left and right, and no-flux on the upper and lower boundaries (as well as the top and bottom).

Dissolved O_2 concentrations measured on waters pumped from Well 304 and simulated using Case 1 and Case 2 parameter sets are shown in Figure 10. Note that Case 2 with a larger apertures and much higher permeability fits fairly well the dissolved O_2 concentrations, assuming initial equilibration with air at 10.5 °C. The unexpected bump to higher concentrations after the system was changed to recirculating water rather than injected tank water, was likely due to some experimental problems while the valves were shut off. This increase and the sharp drop in ^{222}Rn activity at the same time (Figure 11) were captured assuming the pumping and injection were turned off for 10 minutes, allowing just groundwater flow to carry the upstream concentrations into the pumping well.

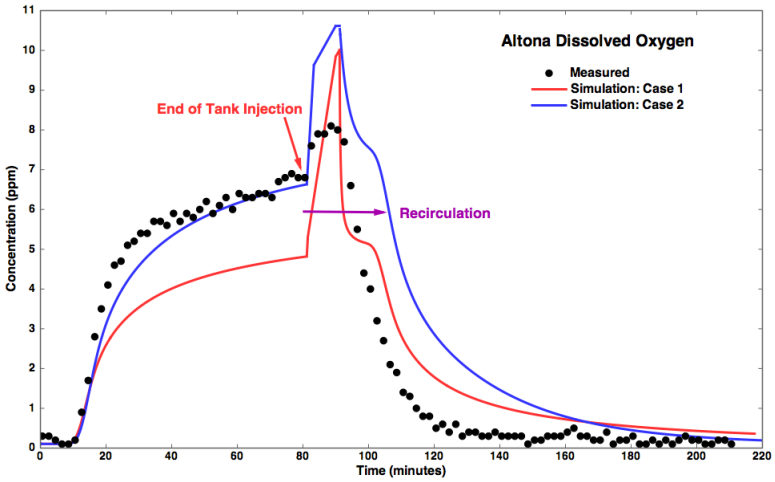

Figure 10: Dissolved O_2 concentrations measured on pumped waters (Well 304) and simulated using Case 1 and Case 2 parameters sets.

^{222}Rn activities measured on waters pumped from Well 304 and simulated using Case 1 and Case 2 parameter sets are shown in Figure 11. Note that the Case 2 parameters give lower ^{222}Rn activities than those for Case 1, even though the simulated dissolved O_2 concentrations fit the observed values much better than Case 1 parameters. The recirculation period assumed the initial groundwater composition has a ^{222}Rn activity of 2200 pCi/liter, so the later activities are likely elevated relative to re-circulated water.

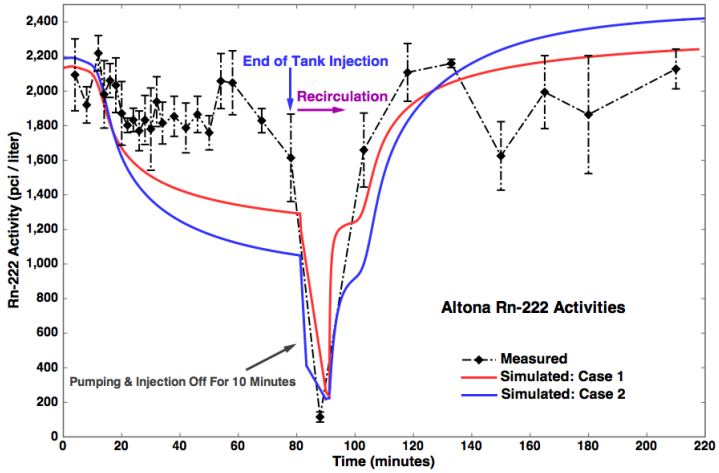

Figure 11: ^{222}Rn activities measured on pumped waters (Well 304) and simulated using Case 1 and Case 2 parameter sets.

It may be possible to find a set of parameters that would match the ^{222}Rn activities and dissolved O_2 concentrations, without having to invoke radium accumulation by sorption, and locally enhanced radon activities. However, the near constant ^{222}Rn in the pumped waters, while showing near conservative behavior for O_2 (aq), suggests that the system is more complex than simply described by ^{222}Rn accumulation in the low porosity rock matrix, and diffusion into flowing fracture fluids. Much better constraints on the system will be possible once detailed characterization of the fracture surface chemistry are performed as well as additional measurements from other wells to test the hypothesis of a ^{222}Rn activity gradient from the lake to the well field.

6. CONCLUSIONS

Our field experiment at Altona demonstrates that ^{222}Rn produced from fractured rocks can be quantified during tracing tests, showing promise for future experiments at larger scales. We have found that small field-scale present complexities, in particular at Atona the large velocity of fluid flow compared to the spatial scale of the well field, that we expect will be distinct from larger natural or stimulated systems where fluid velocities would likely be slower relative to the scale of the fracture system. Reactive transport modeling of our experiment at Altona was able to come to a consistent result that supports previous observations of fracture aperture. However, the anomalously persistent ^{222}Rn concentrations observed in the first portion of the July 28th experiment is not captured by the model, and indicates a secondary source of ^{222}Rn accessed during the experiment. Possibilities include transient contributions from vertical stagnant fractures, or pumping from the matrix due to pressure transients during the experiment. Further refinement and resolution will require spatial characterization of the concentration distribution of the parent(s) of ^{222}Rn, an important factor for improving all models involving ^{222}Rn for fracture characterization.

7. ACKNOLEDGMENTS

Funding for this research was granted to LBNL by the U.S. Dept. of Energy, Office of Energy Efficiency and Renewable Energy, Geothermal Technologies Program. We also wish to thank the William H. Miner Agricultural Research Institute for providing access to the Altona Flat Rock site and for accommodations.

REFERENCES

Becker, M. W., and G.P. Tsoflias (2010), Comparing flux-averaged and resident concentration in a fractured bedrock using ground penetrating radar, Water Resources Research, 46, *W09518,* doi:10.1029/2009WR008260.

Brown, S. T., Kennedy, B. M., DePaolo, D. J., Hurwitz, S., & Evans, W. C. (2013). Ca, Sr, O and D isotope approach to defining the chemical evolution of hydrothermal fluids: Example from Long Valley, CA, USA. *Geochimica Et Cosmochimica Acta*, *122*, 209–225.

DePaolo, D. J. (2006). Isotopic effects in fracture-dominated reactive fluid–rock systems. *Geochimica Et Cosmochimica Acta*, *70*(5), 1077–1096. http://doi.org/10.1016/j.gca.2005.11.022

Hawkins, A. J., D. Fox, M. Becker, and J. Tester (2016), Meso-Scale Field Testing of Reactive Tracers in a Model Geothermal Reservoir, Stanford Geothermal Workshop, 1–16.

Nelson, P. H., Rachiele, R., & Smith, A. (1983). Transport of radon in flowing boreholes at Stripa, Sweden. *Journal of Geophysical Research: Solid Earth (1978–2012)*, *88*(B3), 2395–2405. http://doi.org/10.1029/JB088iB03p02395

Olcott, P., G. (1995), Ground Water Atlas of the United States. Reston, Virgina.

Porcelli, Donald, and Peter W. Swarzenski. "The behavior of U-and Th-series nuclides in groundwater." In *Reviews in Mineralogy and Geochemistry* 52.1 (2003): 317-361.

Rayburn, J. A., P. L. K. Knuepfer, and D. A. Franzi (2005), A series of large, Late Wisconsinan meltwater floods through the Champlain and Hudson Valleys, New York State, USA, Quaternary Science Reviews*,* 24, 2410-2419.

Talley, J., G. S. Baker, M. W. Becker, and N. Beyrle (2005), Four dimensional mapping of tracer channelization in subhorizontal bedrock fractures using surface ground penetrating radar, Geophysical Research Letters*,* 32, doi:10.1029/2004GL021974.

Torgersen, T., J. Benoit, and D. Mackie (1990), Controls on groundwater Rn-222 concentrations in fractured rock, Geophysical Research Letters, *17*(6), 845–848.

Vinson, D. S., A. Vengosh, D. Hirschfeld, and G. S. Dwyer (2009), Relationships between radium and radon occurrence and hydrochemistry in fresh groundwater from fractured crystalline rocks, North Carolina (USA), *Chemical Geology*, *260*(3–4), 159–171.

Wood, W.W., T.F. Kraemer, and A. Shapiro (2004), Radon (222Rn) in groundwater of fractured rocks: A diffusion/ion exchange model, Groundwater, 42(4), 552-567.

Xu, T., N. Spycher, E. Sonnenthal, G. Zhang, L. Zheng, and K. Pruess (2011), TOUGHREACT Version 2.0: A simulator for subsurface reactive transport under non-isothermal multiphase flow conditions, *Computers & Geosciences*, *37*(6), 763–774.